Editors' Suggestion | Featured in Physics

Electric Control of Fermi Arc Spin Transport in Individual Topological Semimetal Nanowires

Ben-Chuan Lin,[1,2,*] Shuo Wang,[1,2,*] An-Qi Wang,[1] Ying Li,[1] Rong-Rong Li,[1] Ke Xia,[2] Dapeng Yu,[2] and Zhi-Min Liao[1,3,†]

[1]*State Key Laboratory for Mesoscopic Physics and Frontiers Science Center for Nano-optoelectronics, School of Physics, Peking University, Beijing 100871, China*

[2]*Institute for Quantum Science and Engineering and Department of Physics, South University of Science and Technology of China, Shenzhen 518055, China*

[3]*Collaborative Innovation Center of Quantum Matter, Peking University, Beijing 100871, China*

(Received 29 September 2019; revised manuscript received 25 November 2019; accepted 28 January 2020; published 16 March 2020)

The exotic topological surface states of Dirac or Weyl semimetals, namely Fermi arcs, are predicted to be spin polarized, while their spin polarization nature is still not revealed by transport measurements. Here, we report the spin-polarized transport in a Dirac semimetal Cd_3As_2 nanowire employing the ferromagnetic electrodes for spin detection. The spin-up and spin-down states can be changed by reversing the current polarity, showing the spin-momentum locking property. Moreover, the nonlocal measurements show a high fidelity of the spin signals, indicating the topological protection nature of the spin transport. As tuning the Fermi level away from the Dirac point by gate voltages, the spin signals gradually decrease and finally are turned off, which is consistent with the fact that the Fermi arc surface state has the maximum ratio near the Dirac point and disappears above the Lifshitz transition point. Our results should be valuable for revealing the transport properties of the spin-polarized Fermi arc surface states in topological semimetals.

DOI: 10.1103/PhysRevLett.124.116802

The combination of topology and condensed matter physics ushered the recent development of the topological physics and topological materials, such as topological insulators [1,2], topological semimetals [3], etc. One of the exotic properties of topological semimetals is the Fermi arc–like topological surface state, which connects the projection points of the Weyl nodes on the surface Brillouin zone [3–13]. The Fermi arc surface states have been predicted to have helical spin-momentum locking property [3,4]. Although this remarkable property has been probed by angle-resolved photoemission spectroscopy [12,13], the spin-polarized transport properties of the topological semimetals have still not been revealed. Moreover, the topological semimetals are conducting both in bulk states and surface states, which makes the surface state detection difficult via transport measurements.

The spin transport in topological insulators [14–18] and more general in materials with spin-momentum locking nature [19–27] has already been extensively investigated. However, the achievement of gate-tunable spin transport, especially the switching effect of the spin signal, is still a challenge. Unlike topological insulators, the topological surface states of Dirac semimetal can be changed to trivial states through the Lifshitz transition [4,28,29]. Such a unique topological transition makes the switching of the spin signal possible, which is promising for the applications of spintronic devices [30,31].

Here, we report the spin transport of the Fermi arc surface states in a Dirac semimetal Cd_3As_2 nanowire. The nanowire with large surface to volume ratio, low carrier density, and gate tunability facilitates the surface states detection. A clear hysteretic loop from the spin-polarized surface states was detected via the ferromagnetic Co electrode. The reverse of spin polarization simply by inverting the current polarity was realized, directly revealing the spin-momentum locking property of the Fermi arc surface states. In the nonlocal measurement configuration, a fully spin-polarized transport was detected. What is more, the spin transport can be completely switched off by a topological phase transition via tuning the Fermi level.

The Cd_3As_2 nanowires grown by chemical vapor deposition method have high crystal quality, large surface-to-volume ratio, and low carrier density [32–34]. The transmission electron microscopy image of a typical nanowire shows its growth along the [112] crystal direction [Fig. 1(a)]. A typical device sketch is presented in Fig. 1(b), and a scanning electron microscopy (SEM) image is shown in Fig. 1(c). The Cd_3As_2 nanowire with diameter ~150 nm was used as the conducting channel. A dc current was applied between the two gold electrodes. The in-plane magnetic field was applied along with the long axis of the cobalt electrode (500 nm wide and 150 nm thick), orthogonal to the current direction. With the ferromagnetic Co electrode as the voltage probe, the measured voltage exhibits a clear hysteretic loop as sweeping the magnetic field at 2 K, as presented in Fig. 1(d). Since there are both bulk and surface states contributing to the total conduction, the background was subtracted to show the potential

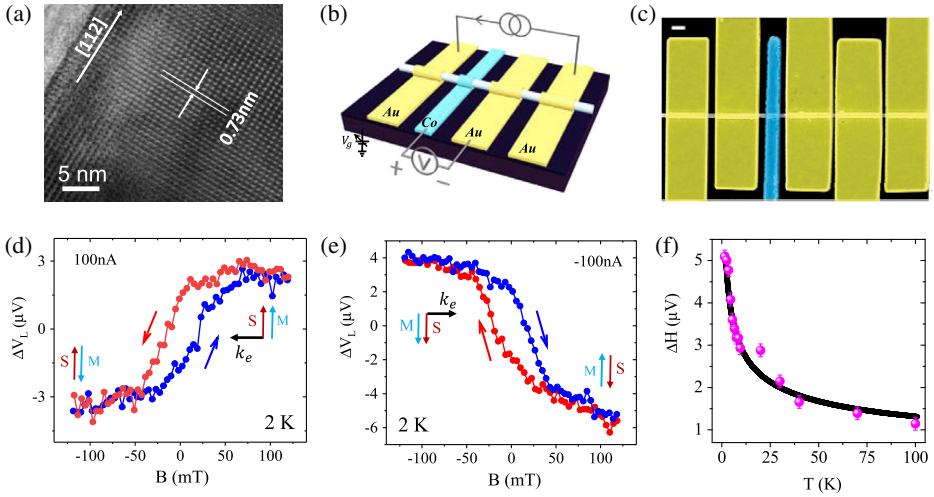

FIG. 1. The local spin transport. (a) The transmission electron microscopy image of a typical Cd_3As_2 nanowire. (b) The device diagram of the spin detection via local measurement. (c) The SEM image of a typical device (false color) with gold electrodes in yellow and a cobalt electrode in blue. Scale bar: 500 nm. (d),(e) The magnetic hysteretic loop measured at 2 K with a direct current of 100 and −100 nA, respectively. The background from the bulk states was subtracted. The electron spin $\boldsymbol{S}$ is right-angle locked with the electron momentum k_e. (f) The temperature dependence of the spin signal in another similar device. The ΔH is defined as the window height at zero magnetic field of the hysteresis loop.

difference (ΔV) of the detected spins of the surface states. A control experiment with gold electrodes deposited as voltage probes was also performed, showing no magnetic hysteretic loops. See the Supplemental Material [35] for experimental details in Figs. S1–S3.

An anticlockwise loop was observed in Fig. 1(d) with a high voltage state for the electron spin $\boldsymbol{S}$ parallel to the Co magnetization $\boldsymbol{M}$ [15] (under positive magnetic field) and a low voltage state for the electron spin $\boldsymbol{S}$ antiparallel to the Co magnetization $\boldsymbol{M}$ (under negative magnetic field). As the current direction reversed, namely −100 nA bias current, the spin orientation of the surface states is also reversed due to the spin-momentum locking. Therefore, there will be a low voltage state under positive magnetic field and a high voltage state under negative magnetic field, forming a clockwise loop, which is consistent with the observation in Fig. 1(e). See the Supplemental Material [35] for detailed analyses of the spin potentiometric measurement in Figs. S4–S5.

Moreover, the hysteretic loop was still clearly observed at 100 K (from another device, in Supplemental Material, Fig. S6) [35], indicating the robustness of the topological surface states. The temperature evolution of the spin signal is presented in Fig. 1(f) as the pink scattered points, which fit well as $\Delta H \propto T^{-0.35}$ by the black line, where the magnetic hysteretic window height is $\Delta H = V(+M) - V(-M)$ and $V(\pm M)$ is the detected voltage at zero magnetic field for different sweeping directions. The power-law behavior of the spin signal can be related with the power-law behavior of the phase coherence length in Cd_3As_2 [39], similar to the behavior of topological surface states in topological insulators [15], where the temperature dependence of the phase coherence length shows similar behavior to the spin signal.

The nonlocal experiment was further conducted, which can greatly reduce the bulk states contribution and single out the topological surface states information. The nonlocal device configuration is depicted in the inset of Fig. 2(a). A direct current of 100 nA was applied to the two adjacent gold electrodes and a voltage was detected between the nonlocal cobalt electrode and gold electrode. The nonlocal cobalt electrode is 350 nm away from the local two electrodes. The nonlocal measurement results are presented as the raw data in Fig. 2 and the signals are symmetric around zero voltage. As shown in Fig. 2(a), a hysteretic loop was observed, indicating that the surface states are topologically protected and immune to the disorders and defects. With the direction of the bias current reversed, the

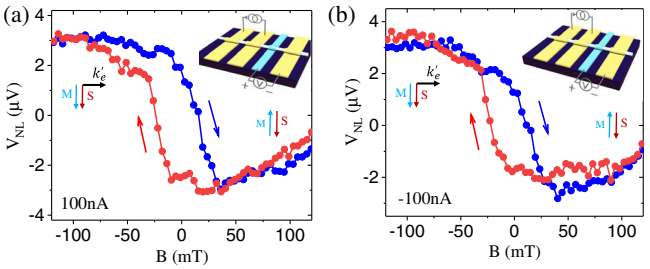

FIG. 2. The nonlocal spin transport at 2 K. (a),(b) The magnetic hysteretic loop measured using the nonlocal configuration depicted in the inset. A direct current ±100 nA was applied. k'_e denotes the electron momentum direction in the nonlocal channel. Apparently the nonlocal spin signals do not change the sign with reversing the source-drain current direction.

hysteretic loop did not change, as shown in Fig. 2(b). Because the nonlocal signals come from carrier diffusion, the nonlocal current flow direction should be the same, that is, from the local to the nonlocal voltage probe. Thus, the spin polarization in the nonlocal channel remains the same direction due to the spin-momentum locking in the whole region.

The spin transport is further tuned by gate voltage V_g, which is applied on the silicon substrate with 285 nm SiO_2 layer. In Fig. 3(a), the local spin signals at different gate voltages were extracted from the raw data (Supplemental Material, Fig. S7) [35] by subtracting the background. The nonlocal spin signals are directly measured and presented in Fig. 3(b). It is obvious that the magnetic hysteretic window height ΔH has the maximum value near the Dirac point -2 V and can be switched off for $V_g > 10$ V or $V_g < -10$ V. It is also worthwhile to note that the nonlocal spin signal value is even larger than the local spin signal [Fig. 3(c)], indicating that the topological surface states have higher spin information fidelity without the current through the bulk states.

We would like to discuss the mechanisms for the spin transport and its gate modulation. The spin-polarized transport from the Rashba effect [40] in this system can be ruled out. First, the spin polarization rate $P \sim 0.73$ is extracted through the hysteretic window height (for details, see the Supplemental Material [35]), which is close to the Fermi arc polarization ($P = 0.8$) observed in the topological semimetal from angle-resolved photoemission spectroscopy results [13]. Second, the Rashba effect is not consistent with the gate voltage dependence. The Rashba field is related to $\boldsymbol{E} \times \boldsymbol{p}$, where $\boldsymbol{p}$ denotes the momentum of the channel carrier and $\boldsymbol{E}$ is the interfacial electric field [41]. Such an interfacial electric field usually has a monotonic gate dependence or is hardly influenced by gate voltage as pinned by metal electrodes [42–47]. In our experiments, however, the gate dependence of the spin signal shows a nonmonotonic behavior and a maximum at the Dirac point. Third, the spin signal should also increase if it comes from the bulk Rashba effect as tuning the Fermi level away from the Dirac point. However, as tuning V_g from the Dirac point to 10 V, the total conductance has a less than twofold increase (Supplemental Material, Fig. S8 [35]), while the nonlocal spin signal decreases over 300 times, which also indicates that the influence of the gate modulated surface-to-volume conductance ratio [47] can also be neglected. Fourth, the Rashba effect induced spin-polarized transport is not likely to result in such a large nonlocal signal without the topological protection. The above analyses jointly rule out the possible Rashba origin.

The gate-tunable spin transport can be well understood in the context of surface Fermi arcs that connect the projections of the bulk Dirac cones on the surface [Fig. 3(d)]. When the Fermi level is near the Dirac point ($V_g = -2V$), the projection of the bulk Dirac cone is a point and the density of state (DOS) of the Fermi arcs reaches the

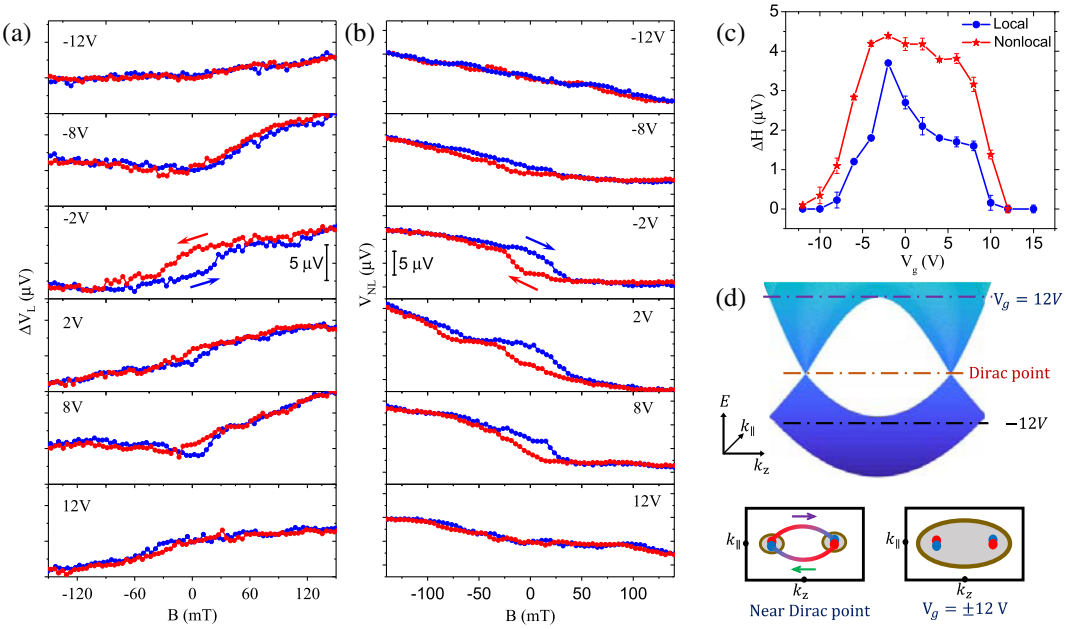

FIG. 3. The field effect of spin signals at 2 K. (a),(b) The V_g tuning of the magnetic hysteretic loops for (a) local and (b) nonlocal measurements. (c) The gate voltage dependence of the window height of the magnetic hysteretic loop extracted from (a),(b). The error bars represent the standard deviations over multiple measurements. (d) The mechanism of the gate-tuned on-off effect of the spin signal. Top: the bulk bands schematic diagram. Bottom: the schematic of surface states. The blue and red dots correspond to different chirality and the arrows denote the spins locked to the momentum. The brown shaded circles denote the Fermi energy pockets. When the Fermi level is above the Lifshitz transition, the two Fermi pockets emerge together, and there are trivial surface states.

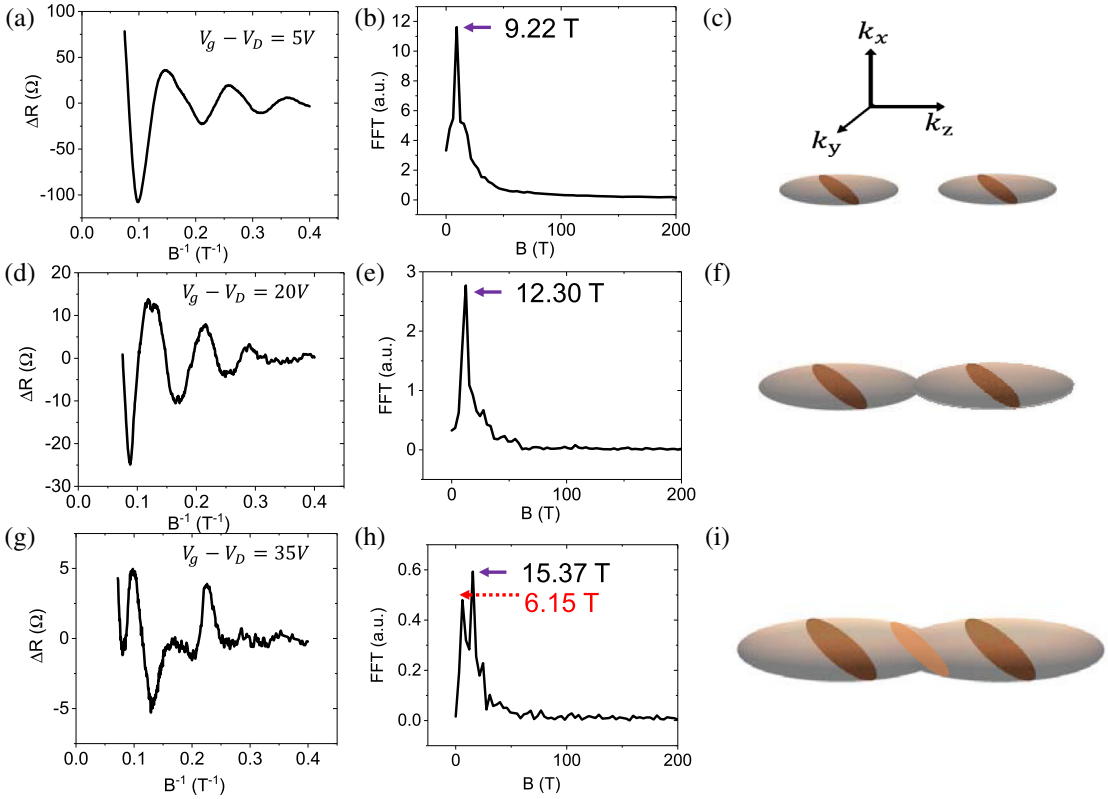

FIG. 4. The Shubnikov–de Haas oscillations at different gate voltages. (a),(d),(g) The SdH oscillations measured with the magnetic field along the nanowire with [112] crystal direction. (b),(e),(h) The fast-Fourier-transform (FFT) analysis. The dual-frequency pattern can be found at high gate voltages in (h). (c),(f),(i) The Fermi surfaces of the Cd_3As_2 at different gate voltages. The k_z axis points towards the [001] direction, along which there are two Dirac points distribution. Under a magnetic field along the [112] direction, the maximum cross section (dark brown) of the Fermi surfaces corresponds to the single SdH frequency. When the Fermi level is above the Lifshitz transition point, the two Fermi surfaces merge together and a minimum cross section (light brown) emerges, see in (i), corresponding to the additional smaller frequency observed.

maximum. Thus, the maximum spin signals can be observed. As tuning the Fermi level away from the Dirac point, the projections of the bulk Dirac cone on the surface are enlarged, and the Fermi arc DOS decreases, resulting in the decrease of spin signals. Notably, the spin signals are switched off for $V_g > 10$ V or $V_g < -10$ V (Fig. 3), which implies the Fermi arc related spin transport is completely quenched in these cases. At the critical points, the sudden disappearance of topological spin signals also indicates the emergence of topological phase transition. The gate-triggered phase transition is most likely from the Lifshitz transition [4,28,29].

The Lifshitz transition was further demonstrated through the analysis of the Shubnikov–de Haas (SdH) oscillations in Fig. 4. A magnetic field was applied along the nanowire with [112] crystal direction, which is also the current direction. The standard SdH oscillations were extracted and a single oscillation frequency ~9.22 T was obtained in the FFT analysis. As the Fermi level was increasing, the corresponding single frequency became larger. When the Fermi level reaches a higher level, for example, $V_g - V_D =$ 35 V, a dual-frequency pattern was clearly observed, that is, a pronounced smaller frequency ~6.15 T appears. This additional frequency cannot be ascribed to the Weyl orbit, because the Weyl-orbit-related transport should also exist near the Dirac point rather than only at high gate voltages. The dual-frequency pattern observed here can be explained by the Lifshitz transition. As shown in Fig. 4(c), the two Fermi surfaces are separated when the Fermi level is near Dirac point. The oblique shaded dark-brown ellipse is the maximum cross section when the magnetic field is applied along [112] crystal direction, which has a 54.7° deviation from the [001] crystal direction (k_z axis) [28]. The maximum cross section explains the observed single frequency. When the Fermi level is above the Lifshitz transition point, the two Fermi surfaces merge together [Fig. 4(i)]. Apart from the two identical maximum cross sections (dark brown) of the Fermi surfaces, there is a minimum cross section (light brown) between them, leading to the additional small frequency ~6.15 T.

In summary, we have provided direct evidence of the spin-polarized Fermi arc states in Dirac semimetals by transport measurements. The spin direction reverses with changing current polarity according to the spin-momentum

locking of the topological surface states. A nonlocal configuration has been used to demonstrate the completely spin-polarized transport. The nonlocal spin signals can be completely switched off, owing to a gate-induced topological phase transition of the surface states. Our results provide a deep understanding of the topological surface states of Dirac semimetals. The gate control of Fermi arc spin-polarized transport should be promising for the topological field effect transistors [23–27].

This work was supported by National Key Research and Development Program of China (No. 2016YFA0300802 and No. 2018YFA0703703), and National Natural Science Foundation of China (No. 91964201, No. 61825401, and No. 11774004).

*These authors contributed equally to this work.
†liaozm@pku.edu.cn

[1] M. Z. Hasan and C. L. Kane, Colloquium: Topological insulators, Rev. Mod. Phys. **82**, 3045 (2010).
[2] X.-L. Qi and S.-C. Zhang, Topological insulators and superconductors, Rev. Mod. Phys. **83**, 1057 (2011).
[3] N. P. Armitage, E. J. Mele, and A. Vishwanath, Weyl and Dirac semimetals in three-dimensional solids, Rev. Mod. Phys. **90**, 015001 (2018).
[4] Z. J. Wang, H. M. Weng, Q. Wu, X. Dai, and Z. Fang, Three-dimensional Dirac semimetal and quantum transport in Cd_3As_2, Phys. Rev. B **88**, 125427 (2013).
[5] Z. K. Liu, J. Jiang, B. Zhou, Z. J. Wang, Y. Zhang, H. M. Weng, D. Prabhakaran, S.-K. Mo, H. Peng, P. Dudin, T. Kim, M. Hoesch, Z. Fang, X. Dai, Z. X. Shen, D. L. Feng, Z. Hussain, and Y. L. Chen, A stable three-dimensional topological Dirac semimetal Cd_3As_2, Nat. Mater. **13**, 677 (2014).
[6] Z. K. Liu, B. Zhou, Y. Zhang, Z. J. Wang, H. M. Weng, D. Prabhakaran, S.-K. Mo, Z. X. Shen, Z. Fang, X. Dai, Z. Hussain, and Y. L. Chen, Discovery of a three-dimensional topological Dirac semimetal, Na_3Bi Science **343**, 864 (2014).
[7] T. Liang, Q. Gibson, M. N. Ali, M. Liu, R. J. Cava, and N. P. Ong, Ultrahigh mobility and giant magnetoresistance in the Dirac semimetal Cd_3As_2, Nat. Mater. **14**, 280 (2015).
[8] H. Yi, Z. J. Wang, C. Y. Chen, Y. Shi, Y. Feng, A. Liang, Z. Xie, S. He, X. Dai, Z. Fang, and X. J. Zhou, Evidence of topological surface state in three-dimensional Dirac semimetal Cd_3As_2, Sci. Rep. **4**, 6106 (2015).
[9] L.-X. Wang, C.-Z. Li, D.-P. Yu, and Z.-M. Liao, Aharonov-Bohm oscillations in Dirac semimetal Cd_3As_2 nanowires, Nat. Commun. **7**, 10769 (2016).
[10] S.-Y. Xu, C. Liu, S. K. Kushwaha, R. Sankar, J. W. Krizan, I. Belopolski, M. Neupane, G. Bian, N. Alidoust, T.-R. Chang, H.-T. Jeng, C.-Y. Huang, W.-F. Tsai, H. Lin, P. P. Shibayev, F.-C. Chou, R. J. Cava, and M. Z. Hasan, Observation of Fermi arc surface states in a topological metal, Science **347**, 294 (2015).
[11] P. J. W. Moll, N. L. Nair, T. Helm, A. C. Potter, I. Kimchi, A. Vishwanath, and J. G. Analytis, Transport evidence for Fermi-arc-mediated chirality transfer in the Dirac semimetal Cd_3As_2, Nature (London) **535**, 266 (2016).
[12] B. Q. Lv, S. Muff, T. Qian, Z. D. Song, S. M. Nie, N. Xu, P. Richard, C. E. Matt, N. C. Plumb, L. X. Zhao, G. F. Chen, Z. Fang, X. Dai, J. H. Dil, J. Mesot, M. Shi, H. M. Weng, and H. Ding, Observation of Fermi-Arc Spin Texture in TaAs, Phys. Rev. Lett. **115**, 217601 (2015).
[13] S.-Y. Xu*et al.*, Spin Polarization and Texture of the Fermi Arcs in the Weyl Fermion Semimetal TaAs, Phys. Rev. Lett. **116**, 096801 (2016).
[14] C. H. Li, O. M. J. van't Erve, J. T. Robinson, Y. Liu, L. Li, and B. T. Jonker, Electrical detection of charge-current-induced spin polarization due to spin-momentum locking in Bi_2Se_3, Nat. Nanotechnol. **9**, 218 (2014).
[15] J. Tang, L.-T. Chang, X. Kou, K. Murata, E. S. Choi, M. Lang, Y. Fan, Y. Jiang, M. Montazeri, W. Jiang, Y. Wang, L. He, and K. L. Wang, Electrical detection of spin-polarized surface states conduction in $(Bi_{0.53}Sb_{0.47})_2Te_3$ topological insulator, Nano Lett. **14**, 5423 (2014).
[16] Y. Ando, T. Hamasaki, T. Kurokawa, K. Ichiba, F. Yang, M. Novak, S. Sasaki, K. Segawa, Y. Ando, and M. Shiraishi, Electrical detection of the spin polarization due to charge flow in the surface state of the topological insulator $Bi_{1.5}Sb_{0.5}Te_{1.7}Se_{1.3}$, Nano Lett. **14**, 6226 (2014).
[17] A. Dankert, J. Geurs, M. V. Kamalakar, S. Charpentier, and S. P. Dash, Room temperature electrical detection of spin polarized currents in topological insulators, Nano Lett. **15**, 7976 (2015).
[18] Y. Fan, P. Upadhyaya, X. Kou, M. Lang, S. Takei, Z. Wang, J. Tang, L. He, L.-T. Chang, M. Montazeri, G. Yu, W. Jiang, T. Nie, R. N. Schwartz, Y. Tserkovnyak, and K. L. Wang, Magnetization switching through giant spin-orbit torque in a magnetically doped topological insulator heterostructure, Nat. Mater. **13**, 699 (2014).
[19] S.-T. Lo, C.-H. Chen, J.-C. Fan, L. W. Smith, G. L. Creeth, C.-W. Chang, M. Pepper, J. P. Griffiths, I. Farrer, H. E. Beere, G. A. C. Jones, D. A. Ritchie, and T.-M. Chen, Controlled spatial separation of spins and coherent dynamics in spin-orbit-coupled nanostructures, Nat. Commun. **8**, 15997 (2017).
[20] S. Sayed, S. Hong, and S. Datta, Transmission-Line Model for Materials with Spin-Momentum Locking, Phys. Rev. Applied **10**, 054044 (2018).
[21] S. Sayed, S. Hong, and S. Datta, Multi-terminal spin valve on channels with spin-momentum locking, Sci. Rep. **6**, 35658 (2016).
[22] J. Lee, H. Kim, J. Chang, S. H. Han, H. C. Koo, S. Sayed, S. Hong, and S. Datta, Multi-terminal spin valve in a strong Rashba channel exhibiting three resistance states, Sci. Rep. **8**, 3397 (2018).
[23] S. Datta and B. Das, Electronic analog of the electro-optic modulator, Appl. Phys. Lett. **56**, 665 (1990).
[24] H. C. Koo, J. H. Kwon, J. Eom, J. Chang, S. H. Han, and M. Johnson, Control of spin precession in a spin-injected field effect transistor, Science **325**, 1515 (2009).
[25] S. Sugahara and J. Nitta, Spin-transistor electronics: An overview and outlook, Proc. IEEE **98**, 2124 (2010).
[26] P. Chuang, S.-C. Ho, L. W. Smith, F. Sfigakis, M. Pepper, C.-H. Chen, J.-C. Fan, J. P. Griffiths, I. Farrer, H. E. Beere, G. A. C. Jones, D. A. Ritchie, and T.-M. Chen, All-electric

all-semiconductor spin field-effect transistors, Nat. Nanotechnol. **10**, 35 (2015).

[27] M. Cahay, Closer to an all-electric device: Spin transistors, Nat. Nanotechnol. **10**, 21 (2015).

[28] S. Jeon, B. B. Zhou, A. Gyenis, B. E. Feldman, I. Kimchi, A. C. Potter, Q. D. Gibson, R. J. Cava, A. Vishwanath, and A. Yazdani, Landau quantization and quasiparticle interference in the three-dimensional Dirac semimetal Cd_3As_2, Nat. Mater. **13**, 851 (2014).

[29] Y. Zhao, H. Liu, C. Zhang, H. Wang, J. Wang, Z. Lin, Y. Xing, H. Lu, J. Liu, Y. Wang, S. M. Brombosz, Z. Xiao, S. Jia, X. C. Xie, and J. Wang, Anisotropic Fermi Surface and Quantum Limit Transport in High Mobility Three-Dimensional Dirac Semimetal Cd_3As_2, Phys. Rev. X **5**, 031037 (2015).

[30] X. Qian, J. Liu, L. Fu, and J. Li, Quantum spin Hall effect in two-dimensional transition metal dichalcogenides, Science **346**, 1344 (2014).

[31] J. Maciejko, E.-A. Kim, and X.-L. Qi, Spin Aharonov-Bohm effect and topological spin transistor, Phys. Rev. B **82**, 195409 (2010).

[32] C.-Z. Li, L.-X. Wang, H. Liu, J. Wang, Z.-M. Liao, and D.-P. Yu, Giant negative magnetoresistance induced by the chiral anomaly in individual Cd_3As_2 nanowires, Nat. Commun. **6**, 10137 (2015).

[33] B.-C. Lin, S. Wang, L.-X. Wang, C.-Z. Li, J.-G. Li, D. Yu, and Z.-M. Liao, Gate-tuned Aharonov-Bohm interference of surface states in a quasiballistic Dirac semimetal nanowire, Phys. Rev. B **95**, 235436 (2017).

[34] S. Wang, B.-C. Lin, W.-Z. Zheng, D. Yu, and Z.-M. Liao, Fano Interference between Bulk and Surface States of a Dirac Semimetal Cd_3As_2 Nanowire, Phys. Rev. Lett. **120**, 257701 (2018).

[35] See Supplemental Material at http://link.aps.org/supplemental/10.1103/PhysRevLett.124.116802 for device fabrications and measurements, characterizations of the ferromagnetic electrodes, control experiments with gold electrodes, mechanisms of spin detection and its gate-modulation, and calculation and comparation of spin polarization, which includes Refs. [36–38].

[36] J. Tian, I. Miotkowski, S. Hong, and Y.-P. Chen, Electrical injection and detection of spin-polarized currents in topological insulator Bi_2Te_2Se, Sci. Rep. **5**, 14293 (2015).

[37] J. Tian, I. Childres, H.-L. Cao, T. Shen, I. Miotkowski, and Y.-P. Chen, Topological insulator based spin valve devices: Evidence for spin polarized transport of spin-momentum-locked topological surface states, Solid State Commun. **191**, 1 (2014).

[38] M.-H. Zhang, X.-F. Wang, S. Zhang, Y. Gao, Z.-H. Yu, X.-Q. Zhang, M. Gao, F.-Q. Song, J. Du, X.-R. Wang, L. He, Y.-B. Xu, and R. Zhang, Unique current-direction-dependent ON–OFF switching in $BiSbTeSe_2$ topological insulator-based spin valve transistors, IEEE Electron Device Lett. **37**, 1231 (2016).

[39] L.-X. Wang, S. Wang, J.-G. Li, C.-Z. Li, D. Yu, and Z.-M. Liao, Universal conductance fluctuations in Dirac semimetal Cd_3As_2 nanowires, Phys. Rev. B **94**, 161402(R) (2016).

[40] A. Manchon, H. C. Koo, J. Nitta, S. M. Frolov, and R. A. Duine, New perspectives for Rashba spin-orbit coupling, Nat. Mater. **14**, 871 (2015).

[41] F. Yang, S. Ghatak, A. A. Taskin, K. Segawa, Y. Ando, M. Shiraishi, Y. Kanai, K. Matsumoto, A. Rosch, and Y. Ando, Switching of charge-current-induced spin polarization in the topological insulator $BiSbTeSe_2$, Phys. Rev. B **94**, 075304 (2016).

[42] J. Nitta, T. Akazaki, H. Takayanagi, and T. Enoki, Gate Control of Spin-Orbit Interaction in an Inverted $In_{0.53}Ga_{0.47}As/In_{0.52}Al_{0.48}As$ Heterostructure, Phys. Rev. Lett. **78**, 1335 (1997).

[43] G. Engels, J. Lange, Th. Schäpers, and H. Lüth, Experimental and theoretical approach to spin splitting in modulation-doped $InxGa_{1-x}As/InP$ quantum wells for $B \to 0$, Phys. Rev. B **55**, R1958 (1997).

[44] C.-M. Hu, J. Nitta, T. Akazaki, H. Takayanagi, J. Osaka, P. Pfeffer, and W. Zawadzki. Zero-field spin splitting in an inverted $In_{0.53}Ga_{0.47}As/In_{0.52}Al_{0.48}As$ heterostructure: Band nonparabolicity influence and the subband dependence, Phys. Rev. B **60**, 7736 (1999).

[45] D. Grundler. Large Rashba Splitting in InAs Quantum Wells due to Electron Wave Function Penetration into the Barrier Layers, Phys. Rev. Lett. **84**, 6074 (2000).

[46] J. P. Heida, B. J. van Wees, J. J. Kuipers, T. M. Klapwijk, and G. Borghs. Spin-orbit interaction in a two-dimensional electron gas in a InAs/AlSb quantum well with gate-controlled electron density, Phys. Rev. B **57**, 11911 (1998).

[47] J. S. Lee, A. R. Richardella, D. R. Hickey, K. A. Mkhoyan, and N. Samarth, Mapping the chemical potential dependence of current-induced spin polarization in a topological insulator, Phys. Rev. B **92**, 155312 (2015).